IET Optoelectronics

Special Issue: Selected Papers from Semiconductor and Integrated Optoelectronics (SIOE) 2019

IET Journals
The Institution of Engineering and Technology

Latest advances in optical frequency combs based on quadratic non-linearity

ISSN 1751-8768
Received on 6th June 2019
Revised 11th October 2019
Accepted on 5th February 2020
E-First on 10th March 2020
doi: 10.1049/iet-opt.2019.0078
www.ietdl.org

Barturen Mariana[1,2] ✉, Maglio Benjamin[3,4], Costanzo Caso Pablo Alejandro[2,5,6]

[1]*Instituto de Tecnología, Universidad Argentina de la Empresa, Lima 775, Buenos Aires, Argentina*
[2]*Consejo Nacional de Investigaciones Científicas y Técnicas (CONICET), Argentina*
[3]*School of Physics and Astronomy, Cardiff University, Cardiff, UK*
[4]*Institute for Compound Semiconductors, Cardiff University, Cardiff, UK*
[5]*Telecommunications Department, Instituto Balseiro, UNCuyo-CNEA, Bariloche, Argentina*
[6]*Comisión Nacional de Energía Atómica (CNEA), Argentina*
✉ *E-mail: mbarturen@uade.edu.ar*

Abstract: Second-order non-linear susceptibility (χ^2) is the cause of many non-linear processes in optics including second harmonic generation, sum frequency generation and difference frequency generation. Optical frequency combs based on χ^2, i.e. quadratic frequency combs, hold the promise of reducing the devices power consumption and footprint since χ^2 materials present a stronger non-linearity than χ^3 materials, which suggests that higher efficiencies can be achieved. In this work, we will revisit the latest quadratic combs experimental advances, concerning power threshold, span and wavelength conversion efficiency.

1 Introduction

Nowadays, photonic devices such as polarisers [1, 2], modulators [3, 4], switches [5], frequency combs [6–8] etc. are intensively studied due to their vast field of application in photonics signal processing [9, 10]. Photonic, plasmonic and hybrid systems have been used to build these components [11, 12]. In particular, frequency combs are relevant in diverse fields as optical clocks [13], precision spectroscopy [14–16], ultraviolet and infrared spectroscopy [17–19], precision distance measurement [20] etc.

Frequency combs based on third-order non-linear susceptibility χ^3 exhibit high repetition rate from several GHz to THz, wide span over hundreds of THz [21] and low-power threshold [22, 23].

Second-order non-linear susceptibility χ^2 is intrinsically higher than χ^3, which can help to increase the efficiency of non-linear processes and decrease the power threshold. The phase-matching condition for the three-wave mixing in χ^2 materials does not require anomalous dispersion, as it happens in Kerr, χ^3 materials [24]. This significantly extends the pliancy of the pump source choices and allows the comb generation over a wider spectral range between mid-infrared and ultraviolet.

After the first report of second harmonic generation (SHG) in a whispering gallery mode resonator [25], research became restricted by stability problems that did not allow achievement of stable wide-mode spectra around the pump and signal waves [26]. The first satisfactory experimental realisation of broad frequency combs in a resonator with χ^2 non-linearity has been recently achieved [27, 28].

In this work, we will revisit the latest advances in quadratic frequency combs (QFCs). At first, we will recall the process of formation through cascaded SHG and optical parametric oscillation (OPO). Next, we will revise the phase-matching techniques utilised in QFCs. After this, we will describe a technique that allows control of the frequency separation of the comb lines. Following, we will list the most commonly used non-linear materials and we will describe different resonator designs. Finally, we will explore the state of the art related to comb span, power threshold and wavelength conversion efficiency.

2 QFC generation

As explained in [29], the QFC formation process has two main steps, which are illustrated in Fig. 1. We consider a fundamental pump light at frequency ω.

The first step consists of SHG of the fundamental pump light. Following, OPO of the SH light at 2ω, gives rise to a signal and idler beams at frequencies $\omega \pm \Delta$. Through cascaded effects of SHG and OPO, higher-order sidebands with separation Δ appear, resulting in a primary comb around the initial pump light.

In the second step, the initial pump power is increased, so secondary sidebands with a separation corresponding to one free spectral range appear in the proximity of the original comb. These secondary combs are born because of OPO of the SH of each line belonging to the primary comb. We remark that the SH lights need to surpass a threshold power to initiate OPO. Finally, when the comb clusters are merged establishing a wide span comb.

In the process explained before, the separation Δ is settled by the group velocity dispersion through SHG and OPO. However, other quadratic non-linear processes such as sum frequency generation (SFG) and difference frequency generation (DFG) can complicate the mechanism of the comb growth as theoretically discussed in [30, 31]. In particular, on the first step, SFG of the fundamental pump light with the signal and idler light leads the non-linear loss and, as a consequence, it significantly influences Δ. Starting from the second or later steps of the cascaded SHG–OPO processes, both SFG and DFG contribute to modulate the value of Δ.

3 Phase-matching approaches

The underlying issue in achieving phase matching in QFCs is that the phase of the second harmonic changes with respect to the fundamental, due to the different light speeds in the crystal. In each coherence length $L_c = 2\pi/\Delta k$, where Δk corresponds to the wavenumber bandwidth, the non-linear polarisation waves are shifted in phase by π radians, and the relative phase slips by $\pi/2$. After the first coherence length, the phase enters a regime, where energy is lost from the field. In general, three methods are preferentially chosen to achieve the phase-matching condition:

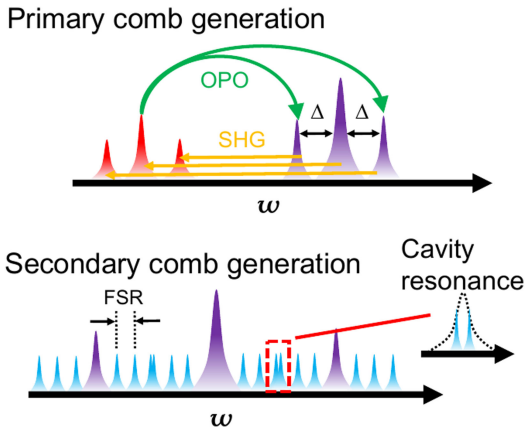

Fig. 1 *Conceptual illustration of the optical comb generation around the fundamental pump light at the 1500 nm band (light violet) and SH light of the pump. The horizontal axis corresponds to angular frequency. While the waveguide only confines the 1.5 μm light, the SH light output has comb structure. Figure extracted from [29]*

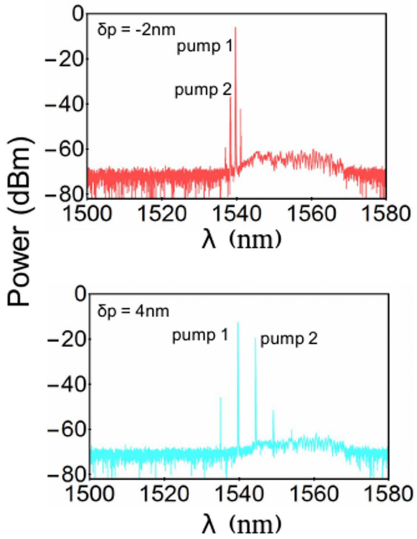

Fig. 2 *Comb separation control by using two pump lights. The pump light at 1540 nm is fixed for all cases. The second pump wavelength is changed from $\lambda_p = -2$ nm to 4 nm. The comb separation corresponds to the wavelength difference λ_p of the two pump lights. Figure extracted from [29]*

quasi-phase matching (QPM), cavity phase matching (CPM) and modal phase matching (MPM).

In QPM, a material with spatially modulated non-linear properties is used. The idea is essentially to allow for a phase mismatch over some propagation distance, and then reverse (or turn off) the non-linear interaction so the involved waves become in phase again. It is not necessary to have different polarisation states of the involved waves; in fact, it is most common to have equal polarisation states (The term 'type-0 phase matching' is sometimes used.). Technologically the growth of such materials does not require forming a stack of thin wafers. A more practical approach is to use ferroelectric crystals forming regions of periodically reversed polarisation domains by applying electric fields; these domains remain intact when the applied field is switched off. The most commonly used material to fabricate quadratic resonators is periodically poled lithium niobate (PPLN). A waveguide made of this material was used for the first demonstration of an on-chip QFC in 2018 [29].

In CPM, the beam travels forward and backwards inside a cavity. The length of the cavity is carefully chosen so that the recirculation of light ensures that the forward and reflected lights are exactly in phase in every circling. QPM requires an engineered microstructure inside the non-linear medium to compensate the phase mismatch by reversing orientation of the non-linear polarisation; while in the case of CPM, the resonance recirculation in the cavity can ensure that the travelling light and reflected light are exactly in phase with every circling. QFCs using CPM have been reported in 2018 [32].

In the MPM scheme, the phase mismatch is compensated by multimode waveguide dispersion. The devices are designed such that the effective indexes of the fundamental modes (TE_{00} and TM_{00}) at 1550 nm are the same as that of higher-order guided modes at 775 nm. This configuration allows the parametric generation of twin photons at 1550 nm, starting from photons at 775 nm in the higher-order mode.

Table 1 Most commonly used non-linear materials and their properties

Material	χ^2, pm/V	Refractive index	Bandgap, eV
LN	−20.6 [33]	$n = 2.28$ [34]	4.9 [35]
GaP	100 [36]	$n = 3.31$ at 637 nm [37]	2.24 [38]
AlN	4.7 [39]	$n = 2.2$ [40]	6.2 [41]

4 Frequency separation control

In [29], beyond the on-chip QFC, the control of the separation of the comb lines was also accomplished. With this aim, two incident beams, with a separation frequency $\delta\omega_p$, were used. The lights are combined before entering the waveguide in such a way that the two incident frequencies are $\omega_p \pm \delta\omega_p/2$. When the two pump lights are injected into the material, SH light is produced at $2\omega_p \pm \delta\omega_p$. Each SH light interacts with their strong subharmonic pump light and, by DFG, new peaks appear at $\omega_p \pm 3\delta\omega_p/2$. The repetition of the cascaded processes generates the comb structure around the pump, with a separation of $\delta\omega_p$, which is defined only by the frequency difference between the incident beams. The experimental results are shown in Fig. 2.

5 Non-linear materials and resonator designs

Table 1 exhibits the properties of some materials widely used in QFC devices: LN, aluminium nitride (AlN) and gallium phosphide (GaP).

All of these compounds possess a large bandgap, which is translated into wideband operation and suppression of the unwanted effect of free carrier absorption.

The most used material is LN since, due to its ferroelectric nature, it enables the fabrication of waveguides with different polarisation domains, which is necessary for QPM. By applying electric fields in different directions, this feature can be easily achieved [42].

On the other hand, AlN is a semiconductor that possesses both strong Kerr χ^3 and Pockel's χ^2 non-linear effects [43]. It has the largest bandgap within the materials described here maximising the advantages explained previously.

Another material used is GaP, which is a semiconductor. The advantage of this compound is that, beyond exhibiting a significant χ^2, it also possesses a high index of refraction compared with AlN or LN, allowing the fabrication of ultra-low-mode volume resonators on a wide variety of substrates.

When the devices have the shape of straight waveguides, they are usually fabricated using a selective coating. For instance, in [29], a high reflective coating for 1500 nm and an anti-reflective coating for its SH light was added at both ends of a PPLN waveguide. In this way, the recirculation of pump light on the cavity was achieved while SH light just went through it, meeting necessary conditions for the CPM process. In the case of microdiscs, no coating is necessary.

6 Comb span and power threshold

When it comes to the power threshold and span of a frequency comb, the quality factor Q plays an intrincated role. On the one hand, a high Q is the key for the intensification of the parametric processes in resonators and, as a consequence, for lowering the power threshold. However, such high Q also increments the

Table 2 Latest achievements in QFC. It is described the pump method, injected power, waveguide, phase-matching technique, quality factor *Q* and span

Reference	Pump method	Injected power	Waveguide	Phase-matching technique	*Q*	Span (3 dB bandwidth)
[28]	modulated CW (pump and probe)	power thr.: 3 mW	GaP microring	anomalous dispersion	2×10^5	100 nm for 1 W power
[44]	CW modulated in wavelength and power	620 mW modulation ratio: 0.6 dB	AlN microring	QPM	7×10^5	64 nm for 620 mW power
[29]	CW 15 kHz linewidth	power thr.: 70 mW	PPLN waveguide	QPM	5.5×10^6	5 nm for 280 mW power
[32]	pulsed wave 10 ns duration 10 Hz repetition rate	power thr.: 9 mW	magnesium oxide-doped LN waveguide	CPM	6.6×10^4	54 nm for 10 mW power
[45]	modulated CW	power thr.: 0.32 mW	single-crystalline LN microdisc	MW resonator resonance equal to optical resonator resonance	1.4×10^8	6 nm for 100 mW MW power 0.32 mW optical power
[46]	CW near infrared	power thr.: 0.35 mW	PPLN box resonator	QPM	2×10^7	20 nm for 9.1 W power

In the phase-matching column, QPM means quasi-phase matching, CPM means cavity phase matching and MPM accounts for modal phase matching. Here, MW stands for microwave.

Table 3 Wavelength conversion efficiency for resonators made of different materials

Reference	Waveguide	Wavelength conversion, nm	Efficiency
[49]	GaP on oxide ring resonator	1550–775	400% $\frac{1}{W}$
[50]	PPLN ridge waveguide	1550–775	240% $\frac{1}{W}$
[51]	epitaxial AlN on sapphire ring resonator	1550–775	17,000% $\frac{1}{W}$

effective non-linear interaction length, reducing the phase-matching bandwidth and making the phase-matching condition tight. Table 2 summarises some of the latest publications regarding QFCs.

In [28, 44], the span is calculated in the 3 dB bandwidth. In the remaining cases, the 3 dB bandwidth span was estimated from plots. The analysed plots were Fig. 2*b* in [29], Fig. 2*a* in [32], Fig. 3*b* in [45] and Fig. 3*b* in [46].

Observing Table 2 it can be seen that the wider spans are achieved in [28, 44].

The wide span achieved in a GaP resonator in [28] is produced by a mixture of χ^2 and χ^3 processes. This is the reason why the phase matching is attained by managing the waveguide dimensions in order to have anomalous dispersion. To measure the χ^3 characteristics of the comb, a modulated pump is employed and a detuned probe scans the comb at an adjacent mode. At sufficiently high frequency, the response is dominated by the Kerr effect (χ^3). At the same time, χ^2 non-linearity enables frequency generation at the SH light. Here, we see how the combination of Kerr and quadratic processes can result in a wide span, low-power threshold comb.

In [44] AlN is explored since it also presents strong χ^3 and χ^2, which make it a very strong candidate for frequency combs without the need of external harmonic generators. In this work, the stabilisation of soliton states inside a ring microresonator is investigated. The principal issue to overcome is that the transition from a chaotic state to a comb state is accompanied by a significant power drop, which induces a blueshift of the cavity resonance through a thermo-optical effect [47, 48]. The proposed solution is a combination of input wavelength and input power modulation. The input wavelength is swept across the resonance at a very high speed while the input power is high at the red side of the resonance and low when going to the blue side. With this technique, the scanning time over the resonance becomes comparable with the time constants of the system and the power drop in the cavity is significantly reduced. This allows stabilisation of the soliton states and a span of 64 nm is achieved with 620 mW input power.

Even though in GaP and AlN resonators, the widest spans have been achieved, their performance is low when compared with LN since in these waveguides a lower power is required to achieve a large span.

Within the group of LN resonators, the widest span is achieved in [32], where the strict phase-matching condition is relaxed by combining techniques. The chosen device is a doubly resonant (pump and SH) Fabri–Perot cavity. The dispersion relation is controlled by temperature to achieve natural phase matching, and then the phase-matching bandwidth is extended through CPM. The power threshold is reached using a pulsed wave of 860 mJ at a frequency of 10 Hz, giving a power around 9 mW. This scheme is shown to be the most effective since it accomplished a wide span with low pump power and low *Q* factor.

Regarding the power threshold, the microdiscs of [45] enabled the lower values within the LN devices group, at the cost of narrower spans.

In [46], a very low-power threshold is also achieved due to the fact of working in the mid-infrared zone (pumping at 1030 nm and measuring SH at 2060 nm), which enables a near-material-limited quality factor.

7 Wavelength conversion efficiency

At last, we analyse the wavelength conversion efficiency. Table 3 presents some of the latest results concerning wavelength conversion efficiency calculated as P_{out}/P_{in}^2, where P_{in} and P_{out} are the input and output powers, respectively.

In GaP resonators, an efficiency of 400% 1/W has recently been achieved [49]. The chosen resonator was a GaP on oxide ring resonator. The elevated refractive index of GaP enables low-mode volume structures. Within these structures, a strong mode overlap is produced facilitating the enhancement of the fundamental and SH modes. A crucial point in achieving high conversion efficiency is the critical coupling of both modes, so in this work, the necessity of an input power coupling region separated from the output power (SH) coupling region, as well as the requirement of optimising both couplings to be critical, are emphasised.

In LN resonators, the highest efficiency reported to our knowledge is 240% 1/W [50]. The resonator consists of a ridge PPLN waveguide, where sub-wavelength dimensions and a low

refractive index substrate (silicon dioxide), allowed high optical confinement and large overlap between the two modes.

Finally, the highest efficiency, 17,000% 1/w, was achieved in an epitaxial AlN on sapphire ring resonator [51]. In this work, a fully etched AlN resonator was fabricated for the first time, minimising power loss and achieving very high efficiency. The input and output coupling regions were also separated in this design.

8 Conclusion

In this work, we have revisited the latest advances in QFCs and have described the principal aspects being the non-linear materials composing the resonators, the comb span and power threshold and the wavelength conversion efficiency.

Concerning the comb span, the cavity phase-matched approach has shown to be the most effective one since it allows extension of the phase-matching bandwidth. The measured comb lines were equidistant within the accuracy of the instruments [32], which suggests the possibility for further active comb stabilisation.

When it comes to the power threshold, the lowest values are close to hundreds of mW, which are of the order of the smallest values reported in Kerr frequency combs [52].

It has been mentioned that incorporating independent coupling regions for the pump and SH lights as well as achieving critical coupling in both of them can dramatically improve the wavelength conversion efficiency.

With respect to Kerr combs based on χ^3 materials, χ^2 combs can be realised all over the transparency range of the non-linear material with less severe constraints on the dispersive characteristics [31].

Capitalising on the intrinsically higher efficiency of second-order processes, χ^2 is expected to help decrease the footprint of integrated photonic devices that have the potential to be more efficient than the χ^3-based counterparts.

9 References

[1] Abadía, N., Saber, M.G., Bello, F., *et al.*: 'CMOS-compatible multi-band plasmonic TE-pass polarizer', *Opt. Express*, 2018, **26**, (23), pp. 30292–30304

[2] Saber, M.G., Abadía, N., Plant, D.V.: 'CMOS compatible all-silicon TM-pass polarizer based on highly doped silicon waveguide', *Opt. Express*, 2018, **26**, (16), pp. 20878–20887

[3] Abadía, N., Bernadin, T., Chaisakul, P., *et al.*: 'Low-power consumption Franz–Keldysh effect plasmonic modulator', *Opt. Express*, 2014, **22**, (9), pp. 11236–11243

[4] Reeves, E., Costanzo-Caso, P., Siahmakoun, A.: 'Theoretical study and demonstration of photonic asynchronous first-order delta–sigma modulator for converting analog input to NRZ binary output', *Microw. Opt. Technol. Lett.*, 2015, **57**, (3), pp. 574–578

[5] Costanzo-Caso, P.A., Gehl, M., Granieri, S., *et al.*: 'Optical bistable switching with symmetrically configured so as in reverse bias', *Microw. Opt. Technol. Lett.*, 2010, **52**, (12), pp. 2753–2759

[6] Erkintalo, M.: 'Widely tunable sidebands and optical frequency combs in passive non-linear resonators'. 2018 Conf. Lasers and Electro-Optics (CLEO), San Jose, CA, USA, 2018, pp. 1–2

[7] Geiselmann, M., Brasch, V., Pfeiffer, M.H., *et al.*: 'Chipscale frequency combs: from soliton physics to coherent telecommunication'. ECOC 2016; 42nd European Conf. Optical Communication, Düsseldorf, Germany, 2016, pp. 1–2

[8] Razeghi, M., Lu, Q., Wu, D., *et al.*: 'Review of high power frequency comb sources based on InP: from MIR to THz at CQD', in (Eds.): '*Terahertz emitters, receivers, and applications IX*', vol. **10756** (International Society for Optics and Photonics, USA, 2018), p. 107560I

[9] Costanzo-Caso, P.A., Siahmakoun, A., Granieri, S.: 'Optical leaky integrator with inverted and non-inverted accumulation', *Microw. Opt. Technol. Lett.*, 2011, **53**, (9), pp. 2034–2037

[10] Rabal, S., Bulus-Rossini, L.A., Costanzo-Caso, P.A.: 'Control strategy of true time delay lines', *Fiber Integr. Opt.*, 2017, **36**, (1–2), pp. 38–58

[11] Abadía, N., Bello, F., Zhong, C., *et al.*: 'Optical and thermal analysis of the light-heat conversion process employing an antenna-based hybrid plasmonic waveguide for HAMR', *Opt. Express*, 2018, **26**, (2), pp. 1752–1765

[12] Kinsey, N., Ferrera, M., Shalaev, V., *et al.*: 'Examining nanophotonics for integrated hybrid systems: a review of plasmonic interconnects and modulators using traditional and alternative materials', *J. Opt. Soc. Am. B*, 2015, **32**, (1), pp. 121–142

[13] Diddams, S.A., Udem, T., Bergquist, J., *et al.*: 'An optical clock based on a single trapped 199hg + ion', *Science*, 2001, **293**, (5531), pp. 825–828

[14] Murphy, M., Udem, T., Holzwarth, R., *et al.*: 'High-precision wavelength calibration of astronomical spectrographs with laser frequency combs', *Mon. Not. R. Astron. Soc.*, 2007, **380**, (2), pp. 839–847

[15] Li, C.H., Benedick, A.J., Fendel, P., *et al.*: 'A laser frequency comb that enables radial velocity measurements with a precision of 1 cm s^{-1}', *Nature*, 2008, **452**, (7187), pp. 610–612

[16] Diddams, S.A., Hollberg, L., Mbele, V.: 'Molecular fingerprinting with the resolved modes of a femtosecond laser frequency comb', *Nature*, 2007, **445**, (7128), pp. 627–630

[17] Gohle, C., Udem, T., Herrmann, M., *et al.*: 'A frequency comb in the extreme ultraviolet', *Nature*, 2005, **436**, (7048), pp. 234–237

[18] Jones, R.J., Moll, K.D., Thorpe, M.J., *et al.*: 'Phase-coherent frequency combs in the vacuum ultraviolet via high-harmonic generation inside a femtosecond enhancement cavity', *Phys. Rev. Lett.*, 2005, **94**, (19), p. 193201

[19] Keilmann, F., Gohle, C., Holzwarth, R.: 'Time-domain mid-infrared frequency-comb spectrometer', *Opt. Lett.*, 2004, **29**, (13), pp. 1542–1544

[20] Coddington, I., Swann, W.C., Nenadovic, L., *et al.*: 'Rapid and precise absolute distance measurements at long range', *Nat. Photonics*, 2009, **3**, (6), pp. 351–356

[21] Kippenberg, T.J., Holzwarth, R., Diddams, S.A.: 'Microresonator-based optical frequency combs', *Science*, 2011, **332**, (6029), pp. 555–559

[22] Barturen, M., Abadía, N., Milano, J., *et al.*: 'Manipulation of extinction features in frequency combs through the usage of graphene', *Opt. Express*, 2018, **26**, (12), pp. 15490–15502

[23] Miller, S.A., Okawachi, Y., Ramelow, S., *et al.*: 'Tunable frequency combs based on dual microring resonators', *Opt. Express*, 2015, **23**, (16), pp. 21527–21540

[24] Buryak, A.V., Di-Trapani, P., Skryabin, D.V., *et al.*: 'Optical solitons due to quadratic non-linearities: from basic physics to futuristic applications', *Phys. Rep.*, 2002, **370**, (2), pp. 63–235

[25] Fürst, J.U., Strekalov, D.V., Elser, D., *et al.*: 'Naturally phase-matched second-harmonic generation in a whispering-gallery-mode resonator', *Phys. Rev. Lett.*, 2010, **104**, p. 153901

[26] Breunig, I.: 'Three-wave mixing in whispering gallery resonators', *Laser Photonics Rev.*, 2016, **10**, (4), pp. 569–587

[27] Herr, S.J., Brasch, V., Szabados, J., *et al.*: 'Frequency comb up- and down-conversion in synchronously driven χ^2 optical microresonators', *Opt. Lett.*, 2018, **43**, (23), pp. 5745–5748

[28] Wilson, D.J., Schneider, K., Hoenl, S., *et al.*: 'Integrated gallium phosphide non-linear photonics', arXiv preprint arXiv:1808.03554, 2018

[29] Ikuta, R., Asano, M., Tani, R., *et al.*: 'Frequency comb generation in a quadratic non-linear waveguide resonator', *Opt. Express*, 2018, **26**, (12), pp. 15551–15558

[30] Leo, F., Hansson, T., Ricciardi, I., *et al.*: 'Walk-off-induced modulation instability, temporal pattern formation, and frequency comb generation in cavity-enhanced second-harmonic generation', *Phys. Rev. Lett.*, 2016, **116**, p. 033901

[31] Mosca, S., Ricciardi, I., Parisi, M., *et al.*: 'Direct generation of optical frequency combs in $\chi^{(2)}$ non-linear cavities', *Nanophotonics*, 2016, **5**, (2), p. 23

[32] Lv, X., Ni, X., Xie, Z., *et al.*: 'Generation of optical frequency comb in a chi-2 sheet micro-optical parametric oscillator via cavity phase matching', arXiv preprint arXiv:1812.06389, 2018

[33] Schiek, R., Pertsch, T.: 'Absolute measurement of the quadratic non-linear susceptibility of lithium niobate in waveguides', *Opt. Mater. Express*, 2012, **2**, (2), pp. 126–139

[34] Zelmon, D.E., Small, D.L., Jundt, D.: 'Infrared corrected Sellmeier coefficients for congruently grown lithium niobate and 5 mol.% magnesium oxide-doped lithium niobate', *J. Opt. Soc. A, B*, 1997, **14**, (12), pp. 3319–3322

[35] Mamoun, S., Merad, A.E., Guilbert, L.: 'Energy bandgap and optical properties of lithium niobate from ab initio calculations', *Comput. Mater. Sci.*, 2013, **79**, pp. 125–131

[36] Dal-Corso, A., Mauri, F., Rubio, A.: 'Density-functional theory of the non-linear optical susceptibility: application to cubic semiconductors', *Phys. Rev. B*, 1996, **53**, (23), p. 15638

[37] Bond, W.: 'Measurement of the refractive indices of several crystals', *J. Appl. Phys.*, 1965, **36**, (5), pp. 1674–1677

[38] Haynes, W.: '*CRC handbook of chemistry and physics 92nd edition CRC press*' (Taylor and Francis, Boca Raton, 2011)

[39] Pernice, W., Xiong, C., Schuck, C., *et al.*: 'Second-harmonic generation in phase-matched aluminum nitride waveguides and micro-ring resonators', *Appl. Phys. Lett.*, 2012, **100**, (22), p. 223501

[40] Pastrňák, J., Roskovcová, L.: 'Refraction index measurements on AlN single crystals', *Phys. Status Solidi (b)*, 1966, **14**, (1), pp. K5–K8

[41] Feneberg, M., Leute, R.A.R., Neuschl, B., *et al.*: 'High-excitation and high-resolution photoluminescence spectra of bulk AlN', *Phys. Rev. B*, 2010, **82**, p. 075208

[42] Miller, G.D., Batchko, R.G., Tulloch, W.M., *et al.*: '42%-efficient single-pass CW second-harmonic generation in periodically poled lithium niobate', *Opt. Lett.*, 1997, **22**, (24), pp. 1834–1836

[43] Xiong, C., Pernice, W.H., Tang, H.X.: 'Low-loss, silicon integrated, aluminum nitride photonic circuits and their use for electro-optic signal processing', *Nano Lett.*, 2012, **12**, (7), pp. 3562–3568

[44] Gong, Z., Bruch, A., Shen, M., *et al.*: 'High-fidelity cavity soliton generation in crystalline AlN micro-ring resonators', *Opt. Lett.*, 2018, **43**, (18), pp. 4366–4369

[45] Rueda, A., Sedlmeir, F., Kumari, M., *et al.*: 'Resonant electro-optic frequency comb', *Nature*, 2019, **568**, (7752), p. 378

[46] Jia, K., Wang, X., Ni, X., *et al.*: 'Mid-infrared optical frequency comb generation from a chi-2 optical superlattice box resonator', arXiv preprint arXiv:1904.00528, 2019

[47] Bao, C., Xuan, Y., Jaramillo-Villegas, J.A., *et al.*: 'Direct soliton generation in microresonators', *Opt. Lett.*, 2017, **42**, (13), pp. 2519–2522

[48] Brasch, V., Geiselmann, M., Pfeiffer, M.H., *et al.*: 'Bringing short-lived dissipative Kerr soliton states in microresonators into a steady state', *Opt. Express*, 2016, **24**, (25), pp. 29312–29320
[49] Logan, A.D., Gould, M., Schmidgall, E.R., *et al.*: '400%/w second-harmonic conversion efficiency in 14 μm-diameter gallium phosphide-on-oxide resonators', *Opt. Express*, 2018, **26**, (26), pp. 33687–33699
[50] Wang, C., Langrock, C., Marandi, A., *et al.*: 'Ultra-high-efficiency wavelength conversion in nanophotonic periodically poled lithium niobate waveguides', *Optica*, 2018, **5**, (11), pp. 1438–1441
[51] Bruch, A.W., Liu, X., Guo, X., *et al.*: '17 000%/w second-harmonic conversion efficiency in single-crystalline aluminum nitride microresonators', *Appl. Phys. Lett.*, 2018, **113**, (13), p. 131102
[52] Shen, X., Beltran, R.C., Diep, V.M., *et al.*: 'Low-threshold parametric oscillation in organically modified microcavities', *Sci. Adv.*, 2018, **4**, (1), p. eaao4507